Environmental Fate of Sulfur in Sulphur Creek, Valles Caldera, New Mexico: Natural Attenuation of Geothermal Components in Affected Watersheds

Daniel J. Lavery, Laura J. Crossey, and Abdul-Mehdi S. Ali
2025, pp. 247-258. https://doi.org/10.56577/FFC-75.247

in:

Geology of the Eastern San Juan Basin - Fall Field Conference 2025, Hobbs, Kevin M.; Mathis, Allyson; Van Der Werff, Brittney;, New Mexico Geological Society 75 th Annual Fall Field Conference Guidebook, 227 p. https://doi.org/10.56577/FFC-75

This page is intentionally left blank to maintain order of facing pages.

New Mexico Geological Society Guidebook, 75th Fall Field Conference, 2025, p. 247–258, https://doi.org/10.56577/FFC-75.247

ENVIRONMENTAL FATE OF SULFUR IN SULPHUR CREEK, VALLES CALDERA, NEW MEXICO: NATURAL ATTENUATION OF GEOTHERMAL COMPONENTS IN AFFECTED WATERSHEDS

DANIEL J. LAVERY[1], LAURA J. CROSSEY[1], ABDUL-MEHDI S. ALI[1]

[1]University of New Mexico Department of Earth and Planetary Science, Northrop Hall, 221 Yale Blvd NE, University of New Mexico, Albuquerque, NM 87131; daniel.lavery@nmt.edu

Abstract—The 1.23-Ma Valles Caldera in north-central New Mexico hosts a young (0.7 Ma to present day) igneous hydrothermal system consistent with the model proposed in Goff and Janik (2000). The Sulphur Springs area within Valles Caldera is an acid-sulfate area typical of this model, discharging acidic waters (pH 1.5–3) formed by oxidation at the surface of magmatic H_2S. We report on samples obtained from springs and streams collected between October 2021 and May 2023 in the Sulphur Creek and Alamo watersheds. Sulphur Creek receives input from Sulphur Springs and exhibits low pH (2–4) and high concentrations of aluminum (≤110 mg/L) and sulfate (≤1,300 mg/L). These hydrothermal components are significantly attenuated by the downstream extent of the field area. This investigation uses geochemical tracers such as major ions and stable and radiogenic isotopes to identify processes controlling attenuation. This research has significance for the continued use of geothermally affected watersheds as water resources.

INTRODUCTION

Volcanic hydrothermal systems discharge thermal waters that can negatively impact water quality of the surface hydrologic system (Nordstrom et al., 2009; McCleskey et al., 2010a, 2010b; Golla, 2019). Hydrothermal systems such as those associated with the Valles Caldera and Yellowstone in Wyoming have been studied by Goff and Janik (2000). Goff et al. (1988) identified the Valles hydrothermal plume as the source of the thermal waters emitted at springs (Soda Dam and Jemez Springs) along the Jemez Fault Zone. McGibbon et al. (2018) extended the reach of the Valles plume down to the Tierra Amarilla warm carbonic springs near San Ysidro, New Mexico. Golla (2019) studied the impacts of thermal springs on the natural salinization of a ~50-km reach of the Jemez River (Fig. 1A). McCleskey et al. (2010a, 2010b) investigated natural attenuation of Yellowstone hydrothermal components in the Gibbon River. The research presented in this paper builds on previous work on the Valles and Yellowstone hydrothermal systems and their effects on surface water quality. The purpose of this research is to determine geochemical and hydrologic factors that control water quality in geothermally affected watersheds. This research also functions to add detail to our understanding of the geochemistry of the Valles acid-sulfate features. We hypothesize that Sulphur Creek naturally attenuates the acid-sulfate geothermal components via dilution and mineral precipitation.

Geologic Background

The 1.23-Ma Valles Caldera in north-central New Mexico is a resurgent dome caldera located at the intersection of the Jemez lineament and the western margin of the Rio Grande rift zone (Smith and Bailey, 1968; Goff and Gardner, 1994; Fig. 2). The Jemez lineament is a northeast-trending chain of volcanic centers spanning from southeast Arizona to northeast New Mexico, of which the Jemez Mountains volcanic field is one (Aldrich, 1986). Tectonic studies of the Colorado Plateau and Rio Grande rift have proposed an origin of Jemez lineament volcanism in a zone of crustal weakness associated with the Yavapai-Mazatzal Proterozoic suture zone (Magnani et al., 2005) that was reactivated during Laramide and post-Laramide tectonic activity (Aldrich and Lauglin, 1984; Aldrich, 1986). Volcanism in the Jemez Mountains is the earliest (~13 Ma) and most voluminous on the Jemez lineament (Goff and Gardner, 1994; Goff and Janik, 2002).

West of the Jemez Mountains is the Sierra Nacimiento, a basement-cored uplift dated to late Campanian age by stratigraphic evidence and apatite fission-track methods (Cather, 2004). The geometry of the Nacimiento fault, which separates the Nacimiento Mountains from the San Juan Basin to the west, is not well constrained. Several possible fault geometries are discussed in Cather (2004).

U.S. Department of Energy Continental Scientific Drilling Program core holes VC-2A and VC-2B (1,762 m depth) provided a window into Jemez Mountains eruptive history and regional stratigraphy in the Sulphur Springs area of the Valles resurgent dome (Gardner et al., 1989). Depth to Precambrian basement (1.42–1.69 Ga; Premo and Kellogg, 2005) in the interior of Valles Caldera is >1,500 m (Gardner et al., 1989). Phanerozoic stratigraphy overlying the basement can be summarized as a sedimentary package ranging in age from Pennsylvanian (Sandia Formation) to Neogene (Santa Fe Group) which is overlain by a complex and voluminous sequence of lavas and tuffs erupted from the Jemez Mountains volcanic field beginning 14 Ma (Gardner et al., 1989; Goff and Gardner, 1994; Kelley et al., 2013). Quaternary landslide and debris flows cover the surface in much of the Sulphur Springs area (Gardner et al., 1989). Detailed drilling reports and stratigraphy from borehole VC-2B can be found in Gardner et al. (1989).

In addition to CO_2 and sulfur gases being emitted from the Valles geothermal system, He-abundance and $^3He/^4He$ composition is consistent with prior studies of Soda Dam, Jemez Springs, and regional studies of the Rocky Mountains that suggest inclusion of deep endogenic fluids in their discharges, indicating a degree of mantle connectivity (Goff and Janik, 2002; Karlstrom et al., 2013). This conclusion is consistent with the setting of the Valles Caldera at the convergence of multiple tectonic zones, the intense fracturing, and a high density of faults within the caldera that allows endogenic fluids to migrate to the surface. Fault control on discharge of discrete and diffuse acid-sulfate waters in the Sulphur Springs area of Valles Caldera is implied by the spatial concentration of springs and fumaroles near mapped surface faults (Fig. 1B).

Hydrothermal Overview

The regional hydrothermal setting of the Valles Caldera is illustrated by the Goff and Janik (2000) model for a volcanic-hosted young igneous system. Sulphur Springs features are representative of the more centrally located acid-sulfate features in this model. The magma body that is the source of heat for the hydrothermal system resides 3–10 km below the surface, corresponding to a low-shear-wave velocity zone (Wilgus et al., 2023).

Three components of the hydrothermal system have been identified from scientific drilling, all separated by low-permeability zones that restrict circulation: an upper vapor zone in the topmost sequences of volcanics and debris flows, and two distinct liquid-dominated zones farther down. One liquid-dominated zone resides in Neogene volcanic rocks and sediments and the other is in a low-permeability fracture zone in the lower Paleozoic section (Gardner et al., 1989; Goff and Gardner, 1994). Hydrothermal fluid temperatures exceeded 200°C in the upper liquid zone and 300°C in the lower liquid zone (Goff and Gardner, 1994).

Hydrothermal fluids convect at depth, but H_2S and H_2O may boil off as the fluid migrates to a shallow depth where the liquid phase converts to a vapor phase that in the Sulphur Springs area is roughly coincident with the 200°C isotherm (Goff and Gardner, 1994). When the gases of the vapor zone condense near the surface, H_2S will oxidize to H_2SO_4 via the following

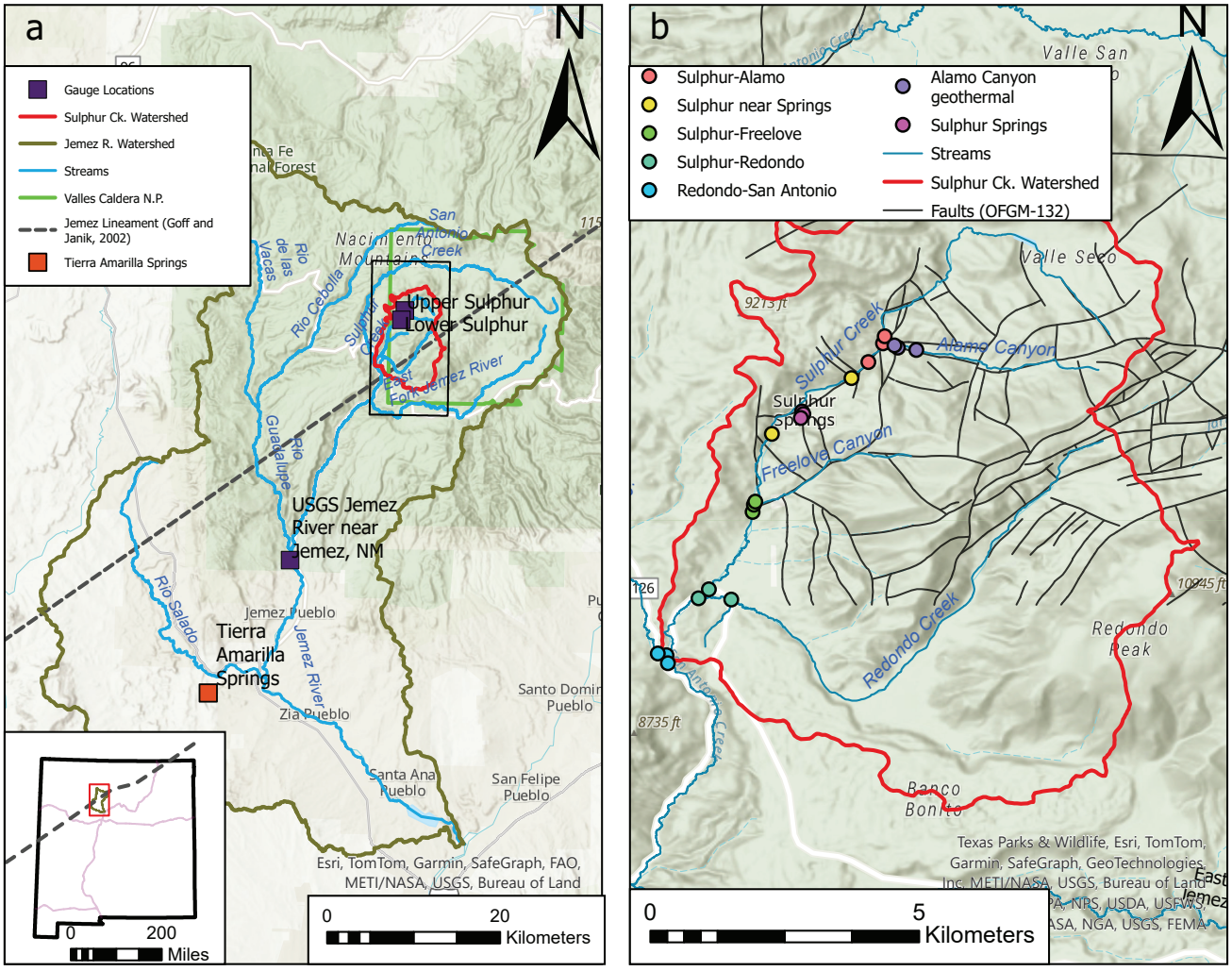

Figure 1. A: Regional major streams and gaging stations of the Jemez River watershed. Outlined in red is the watershed boundary of Sulphur Creek and in green is the administrative boundary of Valles Caldera National Preserve. B: Inset map of the Sulphur Creek watershed with sampling locations, streams, and mapped faults from Goff et al. (2006). Hydrography from U.S. Geological Survey (2022).

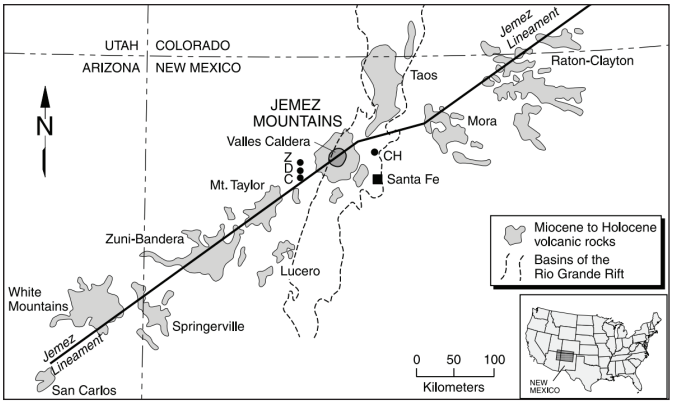

Figure 2. From Goff and Janik (2002), regional tectonic setting of the Valles Caldera at the intersection of the Rio Grande rift western flank and the Jemez lineament.

simplified chain of reactions (Nordstrom et al., 2005), rapidly dropping the fluid pH from circumneutral to pH <3:

$$H^+ + 2HS^- + 2O_2 \rightarrow HS_2O_3^- + H_2O$$

$$H^+ + S_2O_3^{2-} \rightarrow S^0 + HSO_3^-$$

$$HSO_3^- + 0.5O_2 \rightarrow SO_4^{2-} + H^+$$

The geothermal end member at Sulphur Springs can be characterized as warm-to-hot (20° to 90°C), low-pH (pH 1–4), and high-sulfate (SO_4^{2-}; up to 11,000 mg/L) waters with high concentrations of metals derived from leaching of the near-surface material (Goff and Gardner, 1994). Sulfuric geothermal waters alter near-surface landslide and debris flow deposits, with resultant phases including quartz, alunite, gypsum, kaolinite, and unspecified clays (Goff and Gardner, 1994).

Hydrologic Overview

The headwaters of Sulphur Creek lie in the Valle Seco, north of the Valles resurgent dome (Fig. 1B). Sulphur Creek headwaters are fresh and of circumneutral pH. Sulphur Creek receives hydrothermal inputs at the Alamo Creek confluence and, most significantly, in the Sulphur Springs area (Fig. 1B). Downstream of the springs, Sulphur Creek receives moderate pH to circumneutral waters at a variety of confluences (ephemeral Freelove Canyon, Redondo Creek, and Rio San Antonio). Sampling locations for this study are shown in Fig. 1B.

Hydrologic data were assessed over an approximately two-year period from April 2021 to May 2023, encompassing all sampling dates from this project. Stream gages used in this project recorded the highest discharges of the study period in early April 2023, during peak snowmelt. Stream discharge is mainly affected by melting of winter snowpack occurring in the mid-to-late spring and monsoonal precipitation occurring in the mid-to-late summer.

METHODS

Field Methods

Field parameters were measured using an Oakton pH/Con 300 Series pH and conductivity meter. The pH and conductivity probes were calibrated prior to each field excursion (pH 4, 7, 10, and 1413 µS/cm standards, respectively). Field methods for sampling and a description of the sample network can be found in Lavery (2023).

Lab Methods for Major Ions and Stable Isotopes

Alkalinity content for samples was analyzed in the University of New Mexico Diagenesis Lab via a drop-wise pH 4.5 endpoint titration using H_2SO_4. Major ions were analyzed in the University of New Mexico Analytical Chemistry Lab following methods from Hou and Jones (2000) and Jackson (2000). Cations were analyzed by an Optima 5300DV optical emissions spectrometer (ICP-OES). Major anion composition was analyzed on the Thermo Fisher/Dionex Ion Chromatography ISC 1100 ion chromatographer. Stable isotopes of water were analyzed in the University of New Mexico Center for Stable Isotopes using a Picarro L 1102-I Water Isotopic Analyzer, which utilizes cavity ring-down spectroscopy. Stable ^2H (deuterium, D) and ^{18}O analyses followed a method from Wassenaar et al. (2012). Stable isotopic compositions of water are expressed in δ-notation that is shown below:

$$\delta\ (‰) = \left(\frac{R_{sample}}{R_{standard}} - 1\right) * 100$$

Where R_{sample} and $R_{standard}$ are $^{18}O/^{16}O$ or $^2H/^1H$ for the sample and the standard (V-SMOW).

Elemental analysis methods for low-pH samples and method precision can be found in Lavery (2023). Ten percent of the major ion and stable isotope samples were analyzed in duplicate to determine analytical error. Average analytical error was ± 2.5% for cations and ± 5% for anions. Analytical error for $\delta^{18}O$ was approximately ± 0.2‰ and for δD was approximately ± 1.5‰.

Charge Balancing

Charge balancing is a quality control check on major ion composition and was calculated with the following equation:

$$Charge\ balance\ error\ (CBE) = 100 * \frac{\Sigma z_{cat} m_{cat} - \Sigma z_{an} m_{an}}{\Sigma z_{cat} m_{cat} + \Sigma z_{an} m_{an}}$$

where z and m refer to ionic charge and concentration (mol kg^{-1}) of each cation (cat) and anion (an) species, respectively. Adapting a method from Yellowstone geothermal studies (Nordstrom et al., 2009), H^+ was included in charge balancing and total sulfate was distributed between the sulfate and bisulfate species, which improved low-pH charge balancing. Any samples with CBE beyond the ± 10% range after sulfate

modeling underwent geochemical speciation modeling in PhreeqC (Parkhurst, 1999), allowing pH to vary until neutral charge balance was achieved (Table 1).

TABLE 1. Comparison of field-measured pH with modeled pH for low-pH samples.

	pH measurements			
Sample ID	**Field**	**Model**	**ΔpH**	**T (°C)**
DL21-SC	0.97	2.23	1.26	3.8
DL21-SCBSS	0.17	1.97	1.80	1.9
DL21-SCASS	1.87	2.61	0.74	3.7
DL21-SCARC	2.35	2.93	0.58	4.1
DL21-SCTrib	2.24	2.60	0.36	5.7
DL21-SCASS	2.43	2.89	0.46	3.1
DL22-SCARC	2.60	3.46	0.86	10.9
DL22-SCARC2	1.60	3.04	1.44	6.7
DL22-SCARC	1.61	2.99	1.38	6.7
DL22-SCBFC	2.57	2.95	0.38	8.4
DL22-SCBSS	2.54	2.77	0.23	8.5
DL22-ACASC	2.45	3.07	0.62	11.2
DL23-SCARC	3.20	3.00	0.20	12.8
DL23-SCAFC	2.16	2.82	0.66	10.9
DL23-SCBSS	2.00	2.88	0.88	12.8
DL23-MenBH	1.54	2.30	0.76	48.8
DL23-Lemonade	0.84	1.98	1.14	18.5
DL23-ACASC	2.03	2.84	0.81	14.5
DL23-SCAAC	5.43	10.80	5.37	15.8
DL23-SCBAC	2.22	2.91	0.69	13.2

Radiogenic Strontium

Strontium isotopes were analyzed in the University of New Mexico Radiogenic Isotope Laboratory. Filtered acidified water samples (15–25 mL) were spiked with ~1 mL of UNM-Sr2 spike and dried down to a paste, then redissolved in 3N HNO_3 for Eichrom Sr-Spec resin column chemistry. Columns (2 mL) were prepped (0.3 mL of resin), cleaned (18 MΩ water), and conditioned (3N HNO_3). The sample matrix was flushed from the columns with 3N HNO_3, leaving strontium behind in the resin. The strontium was eluted with ultrapure 18 MΩ water, which was then dried down to a powder. The strontium powder was then redissolved in 0.5 mL of 3% HNO_3 for mass spectrometer analysis (Thermo Neptune mc-ICP-MS).

Hydrology

Three gaging stations provided stream discharge values used in this study. The Upper and Lower Sulphur Creek gages are maintained by the National Park Service (Fig. 1B). Precision for these gaging stations was considered to be ± 5% for the duration of this study. The Jemez River at Cañon gaging station is on U.S. Forest Service lands and is maintained by the U.S. Geological Survey (Fig. 1A). This gage was used as an estimator of regional flow conditions. Data were obtained for the 10-year period extending from May 2013 to May 2023 to determine long-term discharge patterns. Data for National Park Service (NPS) Upper and Lower Sulphur Creek gages is provided through the NPS Integrated Resource Management Application (National Park Service, 2023a, 2023b) and the Jemez gage through the USGS Water Dashboard portal (U.S. Geological Survey, 2023).

Geochemical Modeling

The USGS PhreeqC (Parkhurst, 1999) model uses thermodynamic equilibrium calculations for the purpose of understanding likely geochemical speciation and mineral saturation. PhreeqC defaults were used where required constraints were not available.

RESULTS

Field parameters, major ion, and isotope compositions of all samples are reported in supplemental materials.

Field Parameters

Field pH measured in this study varied between pH 1.5 and 7.5. Low pH values generally were from waters in Sulphur Creek downstream of the Alamo Canyon confluence (Fig. 3). Circumneutral samples in the study area were generally located in the Sulphur Creek headwaters and in or downstream of the more dilute confluences (Redondo Creek, Río San Antonio).

Conductivity (µS/cm) measurements were generally low upstream of Sulphur Springs, reached a peak at Sulphur Springs, and decreased downstream of Sulphur Springs (Fig. 3). Conductivity values for samples in this study ranged from 75 µS/cm to >12,000 µS/cm.

Major Ions

Major ions analyzed for these samples were Ca^{2+}, Mg^{2+}, Na^{+}, K^{+}, Cl^{-}, HCO_3^{-}, and total SO_4. Total aluminum, iron, and manganese are also reported. Major ion compositions are reported as total mg/L in Tables S1A–S1C. Measured aluminum concentrations range from below detection to >800 mg/L. Total sulfate concentrations range from 8 mg/L to >11,000 mg/L. Most major ions had their peak concentration at a Sulphur Springs vent, with a few exceptions. Peak chloride concentrations were found in the Redondo Creek drainage. Peak bicarbonate (HCO_3^{-}) concentrations were found in the freshest stream reaches in the study area, as the low pH in the Sulphur Creek watershed meant that the fully protonated carbonate species (H_2CO_3) was favored and therefore were not measured by the methods used in the study.

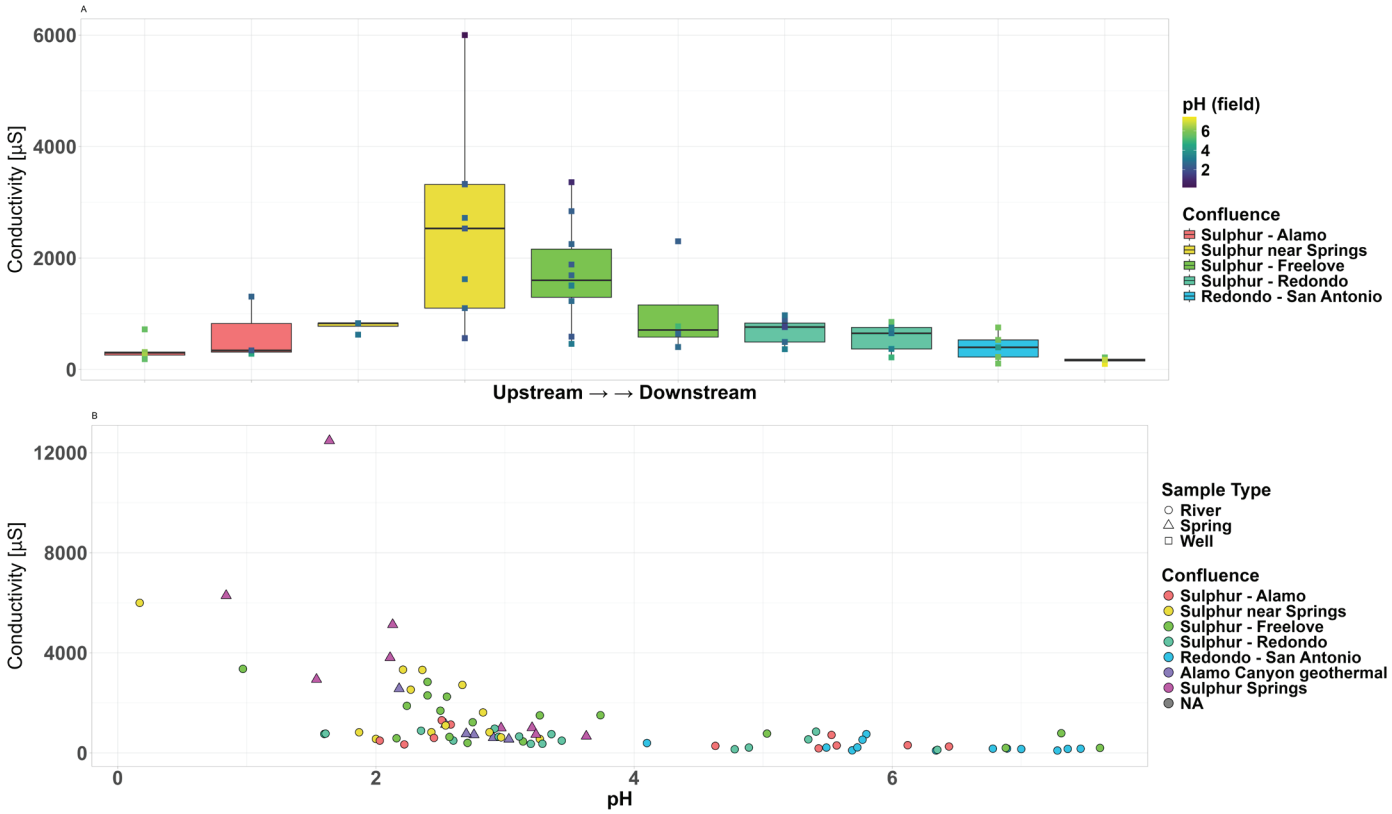

Figure 3. Summation of conductivity and pH relationships. Top: Longitudinal profile describing range of conductivity values (boxplot), color coded by field pH in main-stem stream settings. Bottom: Conductivity-pH scatter relationship showing high conductivity in low-pH samples and lower conductivity in circumneutral samples.

Dissolved Sulfide

Dissolved sulfide (S^{2-}) concentrations of geothermal features ranged from 1.15–1.95 mg/L. Only a small reach of Sulphur Creek (<50 m) immediately adjacent to the Sulphur Springs area had in-stream dissolved sulfide concentrations that were detectable, ranging from 0.06–1.10 mg/L.

Stable Isotopes

$\delta^{18}O$ values for waters ranged from −15‰ to −1‰. δD values ranged from −86‰ to −40‰. Waters are plotted with reference to the global meteoric water line (GMWL) of Craig (1961). Deviations from the GMWL will be discussed later.

Strontium & Strontium isotopes

Strontium concentrations analyzed in the ICP-OES range from <0.01 to 1.87 mg/L (Table 2). From all study samples, eight were selected for strontium isotope analysis. Strontium concentrations for these selected samples were measured again with the mc-ICP-MS during isotopic analysis, ranging from 0.04 to 1.81 mg/L (Table 2). $^{87}Sr/^{86}Sr$ values for these samples ranged from 0.70898 to 0.71111. These isotope ratios are reported to the same precision as other $^{87}Sr/^{86}Sr$ ratios reported from the same lab and instrument (LaPointe et al., 2013; Polyak et al., 2022).

TABLE 2. Sr-isotope analysis results for both ICP-OES and ICP-MS methods. $^{87}Sr/^{86}Sr$ results and 2σ are from ICP-MS.

	Sr-concentration (ppm)			
Sample ID	**ICP-OES**	**ICP-MS**	**$^{87}Sr/^{86}Sr$**	**2σ**
DL22-MenBH	1.9	1.81	0.70834	3.28659E-05
DL22-WomenBH	1.8	1.72	0.71111	2.10481E-05
DL22-Lemonade	0.0	0.04	0.71153	3.49196E-05
DL22-ACWA	0.3	0.34	0.70769	2.20791E-05
DL22-RCASA	0.3	0.28	0.70872	0.00002
DL22-SCBFC	0.6	0.47	0.70882	0.00002
DL22-SCAFC	0.5	0.46	0.70898	2.5239E-05
DL22-FCASC	0.7	0.66	0.70804	0.00002

Geochemical Modeling

Geochemical speciation and saturation modeling for this study was undertaken using USGS PhreeqC (Parkhurst, 1999). Model results are reported in Table S2. Minerals selected for reporting in this study are those aluminum- and/or sulfate-bearing minerals that might attenuate these components.

DISCUSSION

Stable Isotope Chemistry

Stable $\delta^{18}O$ and δD values of sampled waters are shown in Figure 4. Most stream samples fell along the GMWL (Craig, 1961) or the local meteoric water line (LMWL) for the Jemez Mountains (Vuataz and Goff, 1986), indicating meteoric origin for most stream waters. Stable $\delta^{18}O$ and δD values of samples collected corresponded well to values reported in previous studies (Vuataz and Goff, 1986; Szynkiewicz et al., 2012) and extended the range of possible acid-sulfate springs compositions to include isotopically heavier waters. It is possible that either the instrumentation used in analyses in this project or year-to-year variation of hydrologic conditions are responsible for the isotopically heavier waters collected in this study, but these hypotheses were not tested.

Samples collected from Sulphur Springs and a small number of stream samples fell off the LMWL. Selected Sulphur Springs vents (Men's Bathhouse) and stream samples collected in boggy settings (Alamo Canyon) fell below and to the right of the LMWL. This is interpreted as an evaporation effect that resulted in isotopically heavier residual waters (Vuataz and Goff, 1986). Two steam samples (green box in Fig. 4) from the Sulphur Springs area appeared to fall along the evaporation trend to the left of the LMWL. Vuataz and Goff (1986) proposed two potential origins for the steam composition: a two-stage boiling process of deep reservoir fluids (red box in Fig. 4), which would imply that springs compositions originated from isotopic evolution of the condensed steam or boiling of percolating meteoric waters, which would suggest a meteoric origin for the springs compositions.

Two depleted samples collected at the Footbath Spring vent (18–39°C) by Vuataz and Goff (1986) fell off the LMWL by about 10‰. The cooler temperatures at these vents suggests that the $\delta^{18}O$-depletion at these sites was caused by enhanced ^{18}O-fractionation between H_2O and aqueous CO_2 (Vuataz and Goff, 1986). The higher temperatures at the Women's Bathhouse and Lemonade vents suggest their isotopic compositions were more likely related to the evaporation trend seen between the fumarole steam and mudpot samples. One Women's Bathhouse sample from this study overlapped with the range of temperatures (32°C) seen in all Footbath samples, but the magnitude of ^{18}O-depletion of this sample was smaller than those at Footbath, which leaves room for a different process besides CO_2-fractionation affecting the isotopic composition. CO_2 flux at Men's Bathhouse was noticeably higher than at Women's Bathhouse and Lemonade (Smith, 2016), but the proposed fractionation from Vuataz and Goff (1986) relied on lower fluid temperatures to achieve the magnitude of fractionation seen at Footbath Spring. The temperature at Men's Bathhouse in this conceptual model would inhibit CO_2-water fractionation, while the low CO_2-flux at Women's Bathhouse and Lemonade Springs would inhibit fractionation at these vents.

Field Parameters

Each sample in this study was collected alongside a suite of field parameters: pH, temperature, electrical conductivity, and total dissolved solids (TDS). Electrical conductivity and

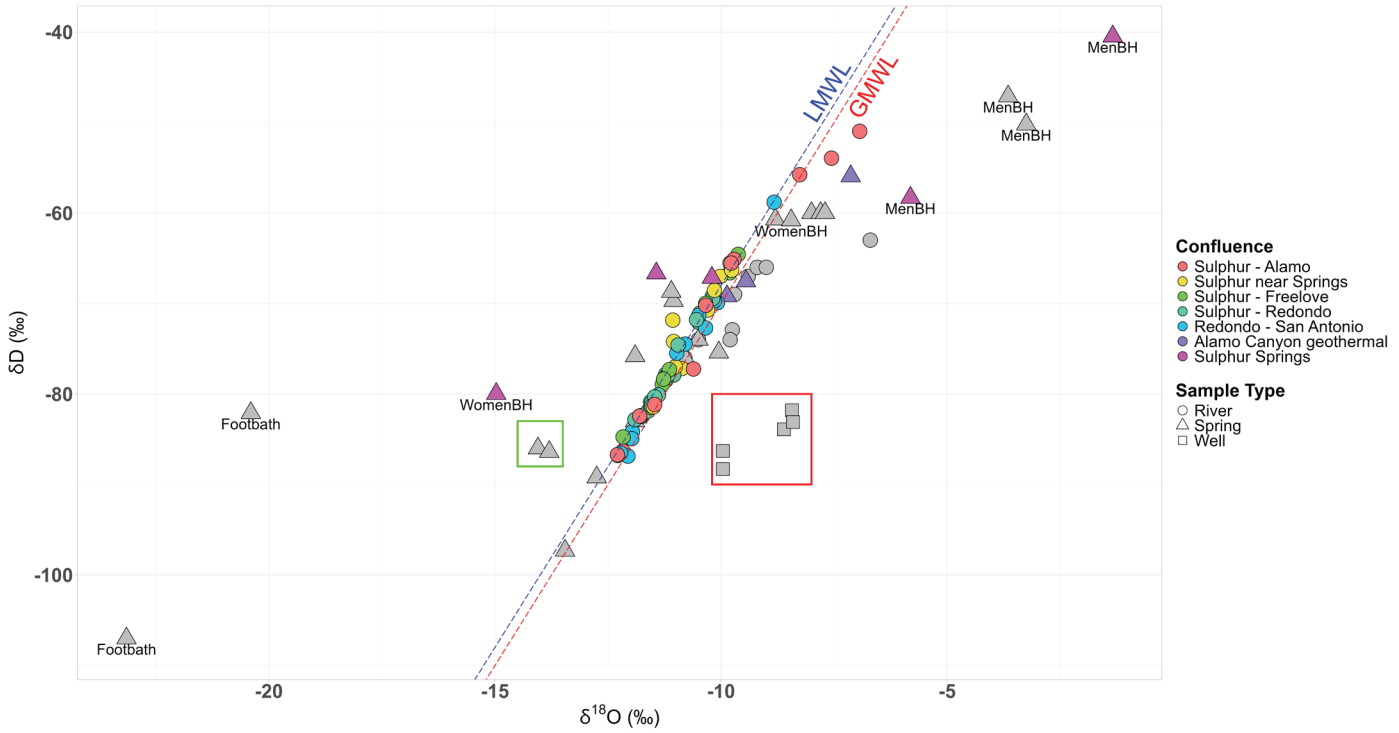

Figure 4. Stable isotopes plot for stream and spring samples in the Sulphur Creek area. Data with gray fill taken from previous studies (Vuataz and Goff, 1986; Szynkiewicz et al., 2012). Colorful fill points sampled in this study. GMWL (red) from Craig (1961b), LMWL (blue) from Vuataz and Goff (1986). Samples from geothermal wells boxed in red, while steam samples of Vuataz and Goff (1986) boxed in green.

pH displayed a negative relationship (Fig. 3). Any process that removes ions from solution (e.g., precipitation, sorption, cation exchange) reduces solution electrical conductivity, as does dilution with fresh water. This negative electrical conductivity-pH relationship illustrates the sum of all ongoing attenuation processes, including dilution.

Aluminum, Sulfate, and Strontium

The following section will discuss the major trends observed in significant geothermal components in the Sulphur Creek watershed. Iron is not included here, but a more in-depth discussion of iron in the Sulphur Creek watershed can be found in Lavery (2023). The deuterium composition of waters was used as a conservative tracer instead of Cl^- as these concentrations increased downstream. Mass loading estimates for the Sulphur Creek watershed and comparisons with estimates from the Yellowstone geothermal system are discussed in more detail in Lavery (2023).

Aluminum

Aluminum is exceptionally sensitive to changes in in-stream pH-conditions. Figure 5 shows the relationship of in-stream aluminum concentrations to pH. Aluminum concentrations were highest at low pH and decreased with increasing pH. Very little aluminum was detectable above pH 4 and none above pH 5.5. Prior studies of aluminum solubility in acidic environments found that it behaves conservatively at pH <4.5 and nonconservatively at pH >5 (Nordstrom and Ball, 1986). Prior studies (Nordstrom and Ball, 1986; Bigham and Nordstrom, 2000; Jones et al., 2011) identified precipitation of crystalline (gibbsite) or amorphous $Al(OH)_3$ phase as controls on aluminum solubility occurring at the first hydrolysis of aluminum:

$$Al^{3+} + H_2O \leftrightarrow AlOH^{2+} + H^+ \ (pK_1 = 5)$$

Geochemical modeling with PhreeqC indicates that only three samples assessed in this study were supersaturated with respect to gibbsite and none with respect to amorphous $Al(OH)_3$ (Table S2). Most samples at pH >5 have aluminum concentrations below detection, which made it difficult to quantify aluminum hydroxide precipitation. However, the shift from conservative to nonconservative aluminum behavior in the pH 4.5–5 transition zone is observed in other acid-sulfate environments (Bigham and Nordstrom, 2000). A denser sampling network in these transitional pH environments would be needed to constrain aluminum behavior in Sulphur Creek.

Since Cl^- increases in downstream samples, δD was used as a conservative tracer for the watershed. For synoptic suites with a full longitudinal suite of data, some interesting trends appeared in the aluminum-δD relationships (Fig. 6). Most aluminum-bearing samples appeared to display conservative mixing trend: where all samples of a triad had measurable aluminum content, the downstream sample tended to fall approximately on a line between the compositions of the upstream samples.

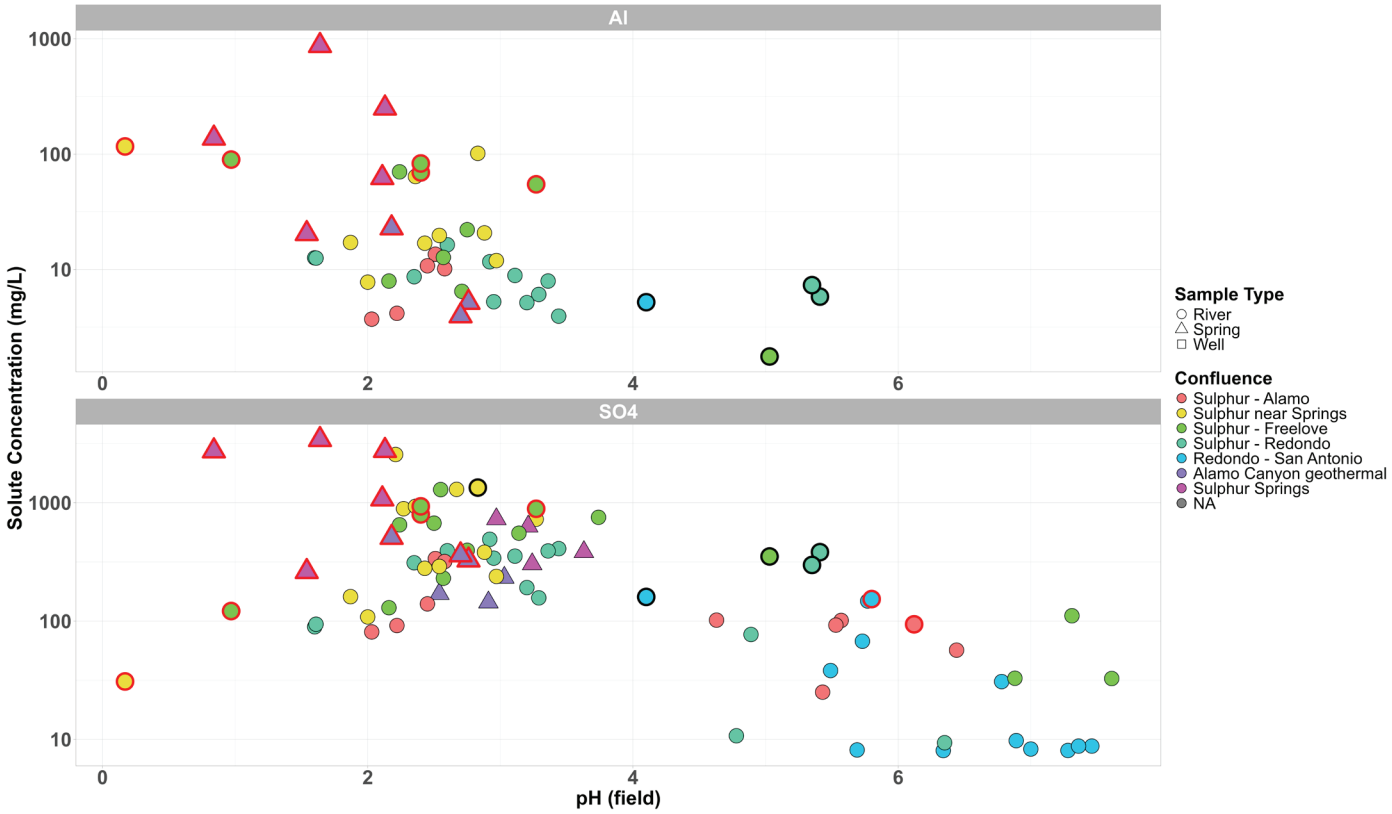

Figure 5. pH plots for selected solutes from samples collected in this study. Red-outlined samples were modeled to be supersaturated with respect to amorphous silica, while boldly outlined samples were modeled to be supersaturated with respect to Al-bearing or SO_4-bearing minerals.

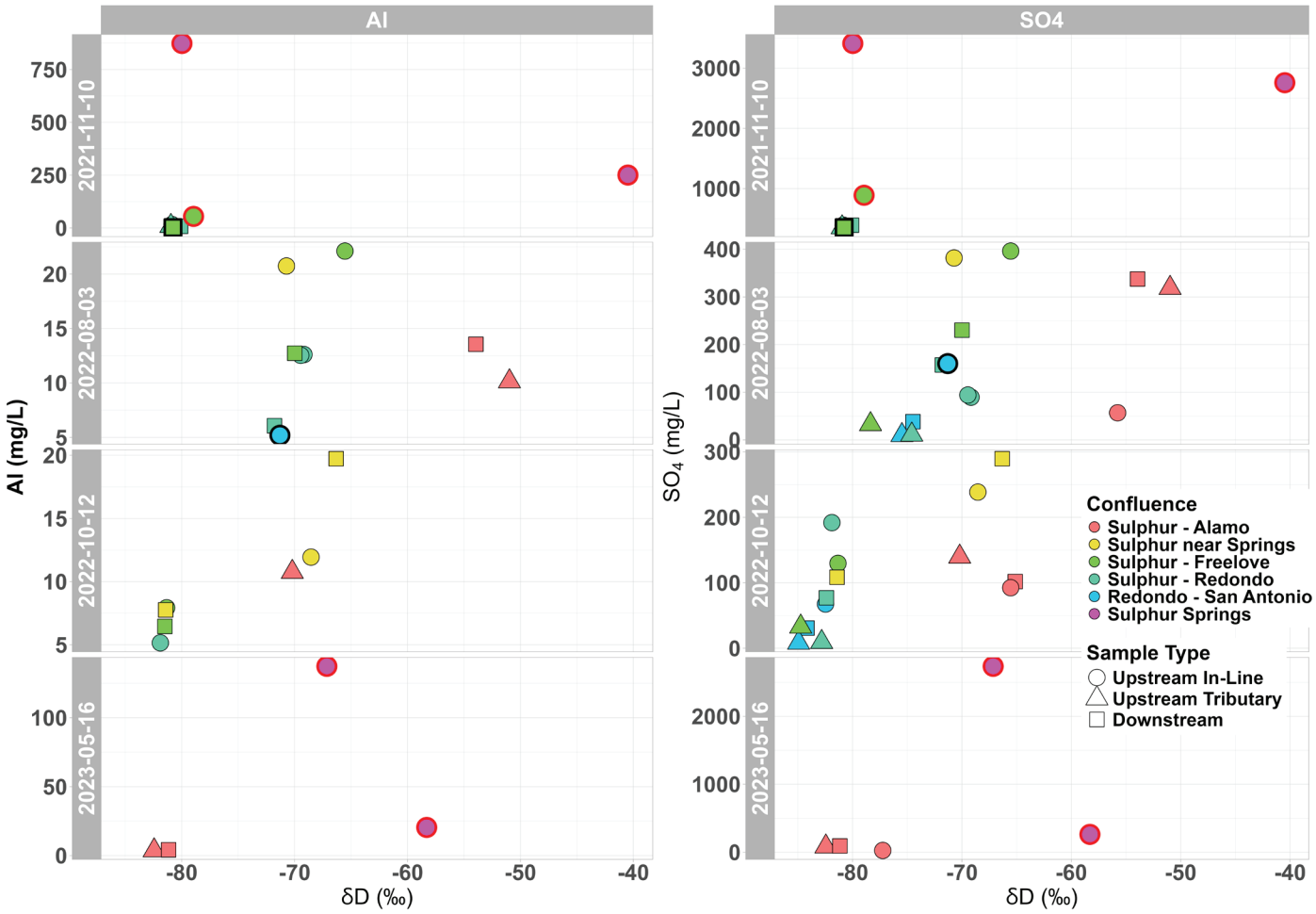

Figure 6. δD plots for selected solutes from samples collected in this study. Red-outlined samples were modeled to be supersaturated with respect to amorphous silica. Boldly outlined samples were modeled to be supersaturated with respect to Al-bearing or SO_4-bearing minerals.

In the August 3, 2022 sampling suite (Fig. 6), the Redondo Creek sample collected above the Sulphur-Redondo confluence was modeled to be supersaturated with respect to alunite and the downstream sample in the triad did not fall cleanly on a line between the two upstream samples, which lent credence to the hypothesis that nonconservative processes occurred at this site on this date. Evaporation-affected waters from Alamo Canyon and waters emitted from Sulphur Springs seemed to be an exception to this pattern.

Sulfate

Sulfate was the primary aqueous anion in the Sulphur Creek system. High sulfate concentrations in this system originated from surface oxidation of magmatic H_2S derived from the Valles magmatic system (Szynkiewicz et al., 2019; Goff and Janik, 2000). Sulfate concentrations in the Sulphur Creek watershed had the highest in-stream levels just downstream of the Sulphur Springs area. Figure 5 shows a plot of log sulfate concentrations versus pH. This is an approximately linear relationship, with sulfate concentrations highest at low pH and lower at circumneutral pH and is related to acidity in the acid-sulfate geothermal system (via the chemical equations shown earlier).

Similar sulfate-δD relationships to aluminum-δD were observed (Fig. 6). The downstream sample at each confluence generally fell between the two upstream samples, indicating conservative mixing at these confluences. However, boldly outlined data points in Figure 6 show samples modeled to be supersatured with respect to alunite. Interestingly, the Redondo-San Antonio cluster for October 12, 2022 contained an upstream sample with model-predicted alunite supersaturation, but the downstream sample fell on a conservative mixing line between the two upstream samples. This could be due to the fact that precipitation occurred in such small amounts to not significantly impact the resulting mixture.

Strontium

Strontium isotopes and concentrations for selected samples are compared in Figure 7. Two samples from Sulphur Springs had $^{87}Sr/^{86}Sr > 0.711$, while the rest (one Sulphur Springs sample and five stream samples from three different confluences) had $^{87}Sr/^{86}Sr < 0.709$. These two values corresponded to strontium isotope ratios found in the Lower Bandelier Tuff pumice and an unspecified rhyolite unit (Vuataz et al., 1988). However, the

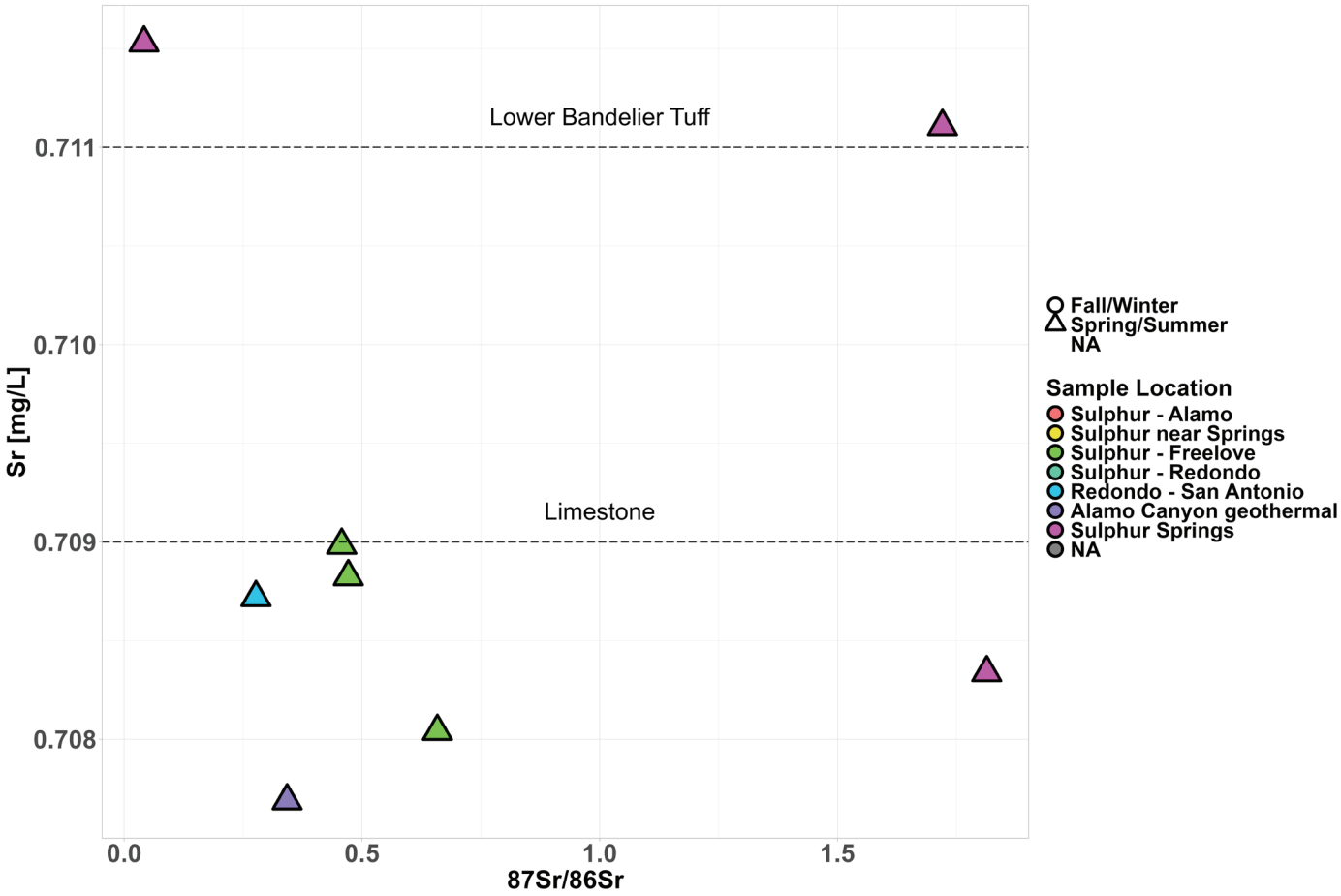

Figure 7. Sr composition of selected waters. $^{87}Sr/^{86}Sr$ for significant Valles lithological units are taken from Vuataz et al. (1988).

Sulphur Springs samples were potentially affected by mixing between waters bearing the strontium signatures of several different rock units. The surface water samples included in the strontium analyses cannot be simply categorized by lithological units as their strontium compositions may be influenced by subsurface and strontium accumulated along surface flow paths. Strontium isotopes for Sulphur Creek waters would require further investigation to determine the source of strontium signatures in surface streams.

Hydrology

Discharge data for the Upper and Lower Sulphur Creek gages for the period of this study were accessed through the NPS IRMA portal (National Park Service, 2023a; National Park Service, 2023b). Discharge peaked during spring snowmelt and late summer monsoonal precipitation. Discharge at these gages for the duration of the study was consistent with 10-year median levels. However, spring 2023 snowmelt led to 10-year maximum discharges in Sulphur Creek and the Jemez River, ranging from 50 to 110 times the 10-year median discharge.

For this study, discharge data were not readily available along the whole length of Sulphur Creek and associated tributaries. Daily average discharge at the Lower Sulphur Creek gage was used as a proxy value for discharge in the field area and compared with in-stream concentrations of aluminum and sulfate on sampling dates (Fig. 8). In Figure 8, discharge data was used to categorize concentrations by general flow conditions in the Sulphur Creek watershed. Samples collected on high-discharge days tended to show lower solute concentrations.

Of the two major contaminants discussed here, sulfate concentrations were most sensitive to discharge. Under a high-flow regime, a larger number of samples in each suite (and therefore a larger stream reach) showed sulfate concentrations below the EPA Secondary Drinking Water Maximum Contaminant Level (SMCL; Environmental Protection Agency, 2023) and low-flow sample suites tended to have more samples above the SMCL (Fig. 8).

Aluminum concentrations were evidently not as closely controlled by discharge. The two highest-flow sample suites showed the smallest spreads of concentration (Fig. 8). Another complication in assessing the role of discharge was analytical. In-stream aluminum concentrations were significantly lower than sulfate concentrations, which meant that higher discharge regimes resulted in more dilute aluminum concentrations, some of which were undetectable or below the standard range for ICP-OES. This reduced the resolution of aluminum data at high discharge as fewer samples showed detectable aluminum concentrations.

Water Quality Implications

The SMCLs for aluminum and sulfate are 0.2 mg/L and 250 mg/L respectively (EPA, 2023). A majority of stream samples collected in this study had aluminum concentrations in excess of the SMCL. At the downstream extent of the field area (Río San Antonio downstream of the Redondo Creek Confluence), very little aluminum remained in solution. However, a majority of samples collected in this study exceeded the aluminum SMCL, regardless of discharge conditions. A significant number of samples fell below the SMCL for sulfate, with the discharge conditions apparently controlling how far upstream the concentrations dropped below SMCL. A greater number of stream samples (and therefore a larger stream reach) fell below the sulfate SMCL under higher discharge regimes (Fig. 8).

The aluminum SMCL of 0.2 mg/L was significantly below the ICP-OES standard range (2.5–10 mg/L) as used in this study. Without accurate low-concentration detection, it was difficult to exactly identify whether aluminum has been attenuated to a level below the SMCL.

CONCLUSIONS

The Sulphur Creek watershed is an example of a self-scrubbing system in which geochemical and hydrologic factors combined to remove selected geothermal components from solution. Changes in pH from mixing with dilute waters was likely responsible for metal attenuation via hydrolysis. Geochemical modeling predicted precipitation of aluminum- and sulfate-bearing minerals, even though these minerals were not observed during field campaigns. However, mineral crusts in the Sulphur Springs area were evident and have been characterized by previous studies (Goff and Gardner, 1994). The role of mixing with dilute fresh water is supported by stable isotope analysis that showed the reduction in sulfate concentrations in selected samples with lower δD (greater meteoric fraction).

Studies from Yellowstone suggest that silica coatings on suspended sediments inhibit sorption as an attenuation process in geothermally affected streams (McCleskey et al., 2010a). Eighteen samples encompassing six different sampling clusters in the Sulphur Creek watershed were predicted to be supersaturated with respect to amorphous silica (Table S2).

Discharge patterns also affected attenuation. Under a low-flow regime, a greater proportion of Sulphur Creek water was derived from acid-sulfate spring water. At higher flows, a greater proportion of Sulphur Creek water was derived from fresh meteoric water and diluted geothermal components more effectively. For less pH-sensitive solutes like sulfate, a clear negative relationship between concentration and discharge appeared, emphasizing dilution in sulfate attenuation. Solutes sensitive to pH like aluminum did not show as clear of a negative relationship, although the range of in-stream concentrations decreased at higher flows.

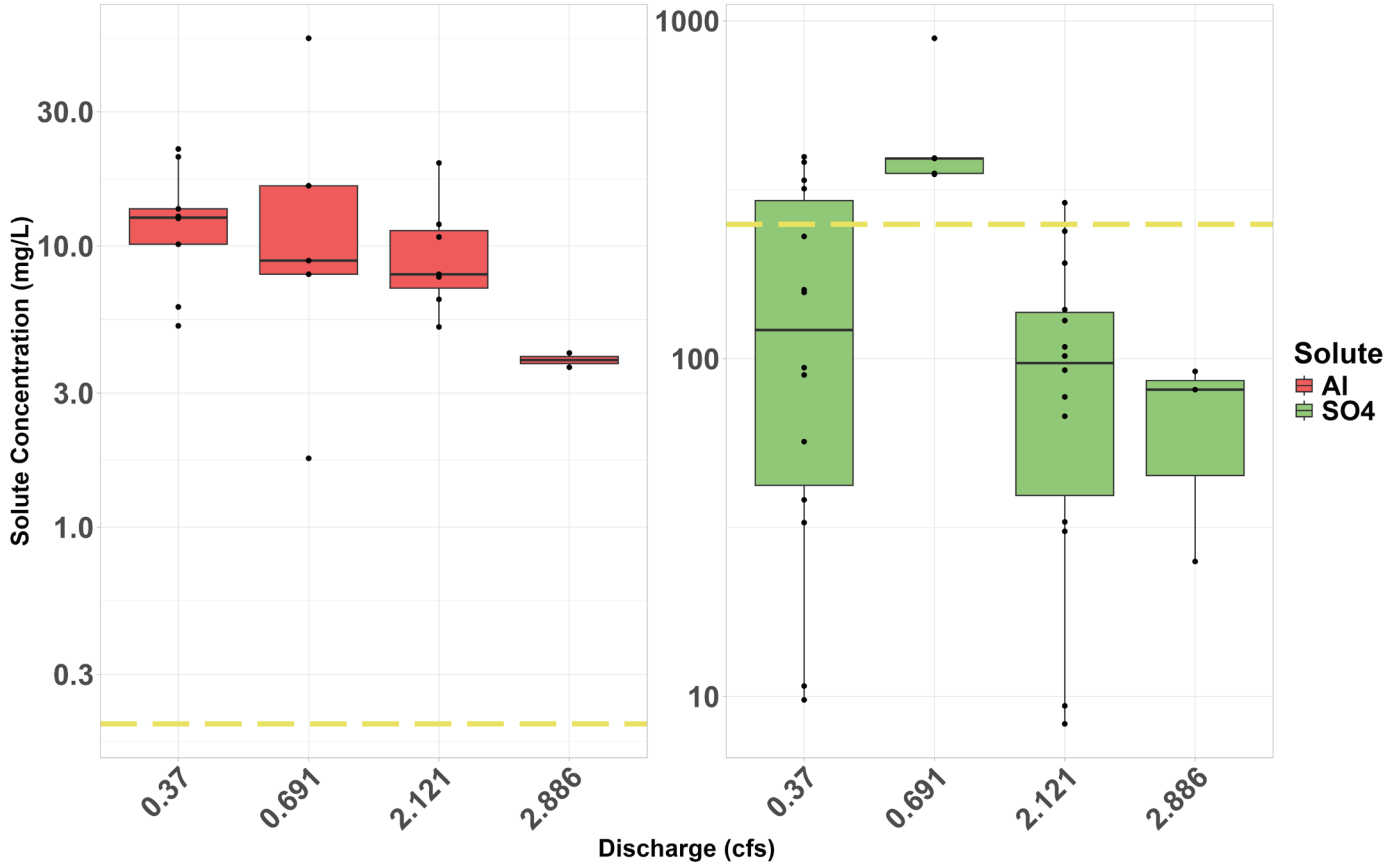

Figure 8. Relationship between discharge at Lower Sulphur gage for and stream composition for selected dates throughout field area. EPA Secondary Drinking Water limits for each solute are displayed as yellow dashed lines (EPA, 2023). Springs samples not considered as they are less impacted by discharge considerations.

ACKNOWLEDGMENTS

Financial support for this project was provided by the New Mexico Water Resources Research Institute (Student Water Grant Q02369), the New Mexico Geological Society (Graduate Grants-in-Aid), the Geological Society of America (Graduate Grants-in-Aid), and the UNM Department of Earth and Planetary Science (Trauger Graduate Scholarship). Dr. Robert Parmenter and Dave Pittenger (Valles Caldera National Preserve) provided access to the Sulphur Springs area and hydrology datasets.

REFERENCES

Aldrich, M.J., 1986, Tectonics of the Jemez lineament in the Jemez Mountains and Rio Grande rift: Journal of Geophysical Research, v. 91, p. 1753–1762. https://doi.org/10.1029/JB091iB02p01753

Aldrich, M.J. and Laughlin, A.W., 1984, A model for the tectonic development of the southeastern Colorado Plateau boundary: Journal of Geophysical Research, v. 89, p. 10207–10218. https://doi.org/10.1029/JB089iB12p10207

Bigham, J.M., and Nordstrom, D.K., 2000, Iron and aluminum hydroxysulfates from acid sulfate waters: Reviews in mineralogy and geochemistry, v. 40, p. 351–403. https://doi.org/10.2138/rmg.2000.40.7

Cather, S.M., 2004, Laramide orogeny in central and northern New Mexico and southern Colorado, *in* Mack, G.H., and Giles, K.A., eds., The Geology of New Mexico, A Geological History: Socorro, New Mexico Geological Society, Special Publication 11, p. 203–248. https://doi.org/10.56577/SP-11

Craig, H., 1961, Isotopic variations in meteoric waters: Science, v. 133, p. 1702–1703. https://doi.org/10.1126/science.133.3465.1702

Environmental Protection Agency, 2023, Secondary drinking water standards: Guidance for nuisance chemicals, 2023: https://www.epa.gov/sdwa/secondary-drinking-water-standards-guidance-nuisance-chemicals (accessed 9 June 2023).

Gardner, J.N., Hulen, J.B., Lysne, P., Jacobson, R., Goff, F., Nielson, D.L., Pisto, L., Criswell, C.W., Gribble, R., Meeker, K., Musgrave, J.A., Smith, T., and Wilson, D., 1989, Scientific core hole Valles Caldera #2b (VC-2B), New Mexico—Drilling and Some initial results: U.S. Office of Scientific and Technical Information Report LA-UR-89-2025, 10 p.

Goff, F. and Gardner, J.N., 1994, Evolution of a mineralized geothermal system, Valles Caldera, New Mexico: Economic Geology, v. 89, p. 1803–1832. https://doi.org/10.2113/gsecongeo.89.8.1803

Goff, F. and Janik, C., 2000, Geothermal Systems, *in* Sigurdsson, H., Houghton, B., Rymer, H., Stix, J., and McNutt, S., eds., Encyclopedia of Volcanoes: San Diego, CA, Elsevier, p. 817–834.

Goff, F. and Janik, C.J., 2002, Gas geochemistry of the Valles caldera region, New Mexico and comparisons with gases at Yellowstone, Long Valley, and other geothermal system: Journal of Volcanology and Geothermal Research, v. 116, p. 299–323. https://doi.org/10.1016/S0377-0273(02)00222-6

Goff, F., Reneau, S.L., Goff, C.J., Gardner, J.N., Drakos, P.G., and Katzman, D., 2006, Geologic map of the Valle San Antonio quadrangle, Sandoval County, New Mexico: New Mexico Bureau of Geology and Mineral Resources Open-File Geologic Map 132, scale 1:24,000. https://doi.org/10.58799/OF-GM-132

Goff, F., Shevenell, L., and Gardner, J.N., 1988, The hydrothermal outflow plume of Valles Caldera, New Mexico, and a comparison with other outflow plumes: Journal of Geophysical Research, v. 93, p. 6041–6058. https://doi.org/10.1029/JB093iB06p06041

Golla, J.K., 2019, Natural salinization of the Jemez River, New Mexico—An insight from trace element geochemistry [M.S. thesis]: Albuquerque, University of New Mexico, 62 p.

Hou, X. and Jones, B. T., 2000, Inductively coupled plasma/optical emission spectrometry, in Meyers, R.A., ed., Encyclopedia of Analytical Chemistry, Chichester, UK, Wiley, p. 9468–9485. doi:10.1002/9780470027318.a5110

Jackson, P.E., 2000, Ion chromatography in environmental analysis, *in* Meyers, R.A., ed., Encyclopedia of Analytical Chemistry, Chichester, UK, Wiley, p. 2279–2801. https://doi.org/10.1002/9780470027318.a0835

Jones, A.M., Collins, R.N., and Waite, D.T., 2011, Mineral species control of aluminum solubility in sulfate-rich acidic waters: Geochimica et Cosmochimica Acta, v. 75, p. 965–977. https://doi.org/10.1016/j.gca.2010.12.001

Karlstrom, K.E., Crossey, L.J., Hilton, D.R., and Barry, P.H., 2013, Mantle ^{3}He and CO_2 degassing in carbonic and geothermal springs of Colorado and implications for neotectonics of the Rocky Mountains: Geology, v. 41, p. 495–498. https://doi.org/10.1130/G34007.1

Kelley, S.A., McIntosh, W.C., Goff, F., Kempter, K.A., Wolff, J.A., Esser, R., Braschayko, S., Love, D., and Gardner, J.N., 2013, Spatial and temporal trends in pre-caldera Jemez Mountains volcanic and fault activity: Geosphere, v. 9, p. 614–646. https://doi.org/10.1130/GES00897.1

LaPointe, Z., Polyak, V., and Asmerom, Y., 2013, Uranium and strontium isotope study of late-stage speleothems from lava tube caves in El Malpais National Monument, New Mexico: New Mexico Geological Society, Guidebook 64, p. 223–228.

Lavery, D.J., 2023, Environmental fate of sulfur in Sulphur Creek, Valles Caldera, NM—Implications for metal transport and water quality [M.S. thesis]: Albuquerque, University of New Mexico, 87 p.

Magnani, M. B., Levander, A., Miller, K. C., Eshete, T., and Karlstrom, K. E., 2005, Seismic Investigation of the Yavapai-Mazatzal Transition Zone and the Jemez Lineament in Northeastern New Mexico, *in* Karlstrom, K.E. and Keller, G.R., eds., The Rocky Mountain Region—An Evolving Lithosphere: Washington, DC, American Geophysical Union, v. 154, p. 227–238.

McCleskey, R.B., Nordstrom, D.K., Susong, D.D., Ball, J.W., and Holloway, J.M., 2010a, Source and fate of inorganic solutes in the Gibbon River, Yellowstone National Park, Wyoming, USA—I. Low-flow discharge and major solute chemistry: Journal of Volcanology and Geothermal Research, v. 193, p. 189–202. https://doi.org/10.1016/j.jvolgeores.2010.03.014

McCleskey, R.B., Nordstrom, D.K., Susong, D.D., and Taylor, H.E., 2010b, Source and fate of inorganic solutes in the Gibbon River, Yellowstone National Park, Wyoming, USA—II. Trace element chemistry: Journal of Volcanology and Geothermal Research, v. 196, p. 139–155. https://doi.org/10.1016/j.jvolgeores.2010.05.004

McGibbon, C., Crossey, L.J., Karlstrom, K.E., and Grulke, T., 2018, Carbonic springs as distal manifestations of geothermal systems, highlighting the importance of fault pathways and hydrochemical mixing—Example from the Jemez Mountains, New Mexico: Applied Geochemistry, v. 98, p. 45–57. doi.org/10.1016/j.apgeochem.2018.08.015

National Park Service, 2023a, Discharge measurements for the Lower Sulphur Creek stream gage from May 24, 2013 to May 24, 2023, Valles Caldera National Park (VALL_LWRSUL): NPS IRMA Portal. https://irma.nps.gov/aqwebportal/Data/DataSet/Export/Location/VALL_LWRSUL/DataSet/Discharge/Discharge/Interval/AllData (accessed 15 May 2023).

National Park Service, 2023b, Discharge measurements for the Upper Sulphur Creek stream gage from May 24, 2013 to May 24, 2023, Valles Caldera National Park (VALL_UPRSUL): NPS IRMA Portal. https://irma.nps.gov/aqwebportal/Data/DataSet/Summary/Location/VALL_UPRSUL/DataSet/Discharge/Discharge/Interval/AllData (accessed 15 May 2023).

Nordstrom, D.K., and Ball., J.W., 1986, The geochemical behavior of aluminum in acidified surface waters: Science, v. 232, p. 54–56. https://doi.org/10.1126/science.232.4746.54

Nordstrom, D., Ball, J.W., and Mccleskey, R., 2005, Ground water to surface water—Chemistry of thermal outflows in Yellowstone National Park, *in* Inskeep, W.P. and McDermott, T.R., eds., Geothermal Biology and Geochemistry in Yellowstone National Park, Bozeman, Montana State University, p. 73–94.

Nordstrom, D.K., McCleskey, R.B., and Ball, J.W., 2009 Sulfur geochemistry of hydrothermal waters in Yellowstone National Park—IV Acid-sulfate waters: Applied Geochemistry, v. 24, p. 191–207. https://doi.org/10.1016/j.apgeochem.2008.11.019

Parkhurst, D.L., 1999. User's guide to PHREEQC—A computer program for speciation, reaction path, advective-transport and inverse geochemical calculations: U.S. Geological Survey Water-Resources Investigations Report 95-4227.

Polyak, V.J., Provencio, P.P., Asmerom, Y., Davis, D.G., Onac, B.P., Palmer, A.N., and Palmer, M.V., 2022, Timing of sulfuric acid speleogenesis (SAS) as an indicator of canyon incision rates of the Shoshone and Bighorn rivers, Wyoming, USA: Geomorphology, v. 410. https://doi.org/10.1016/j.geomorph.2022.108281

Premo, W.R. and Kellogg, K.S., 2005, Timing and origin of Proterozoic basement rocks in the Sierra Nacimiento region, NW New Mexico—Evidence from SHRIMP U-Pb zircon geochronology and Nd isotopic tracer studies: Geological Society of America Abstracts with Programs, vol. 37, no. 6, p. 42.

Smith, J., 2016, CO_2 flux along faults of the central Rio Grande rift, New Mexico [M.S. thesis]: Albuquerque, University of New Mexico, 115 p.

Smith, R.L. and Bailey, R.A., 1968, Resurgent cauldrons, *in* Coats, R.R., Hay, R.L., and Anderson, C.A., eds., Studies in Volcanology, Boulder, Geological Society of America, p. 613–662. https://doi.org/10.1130/MEM116-p613

Szynkiewicz, A., Goff, F., Vaniman, D., and Pribil, M.J., 2019, Sulfur cycle in the Valles Caldera volcanic complex, New Mexico, Letter 1—Sulfate sources in aqueous system, and implications for S isotope record on Gale Crater on Mars: Earth and Planetary Science Letters, v. 506, p. 540–551. https://doi.org/10.1016/j.epsl.2018.10.036

Szynkiewicz, A., Johnson, A.P., and Pratt, L.M., 2012, Sulfur species and biosignatures in Sulphur Springs, Valles Caldera, New Mexico—Implications for Mars astrobiology: Earth and Planetary Science Letters, v. 321–322, p. 1–13. https://doi.org/10.1016/j.epsl.2011.12.015

U.S. Geological Survey, 2022, National hydrography dataset best resolution (nhd) for hydrological unit (HU) 8 – 13020201 (published 12092022) shapefile: https://apps.nationalmap.gov/downloader/ (accessed 13 February 2023).

U.S. Geological Survey, 2023, Discharge measurements for the Jemez River stream gage (USGS 08324000) from April 4, 2021 to May 24, 2023: U.S. Geological Survey National Water Dashboard. https://waterdata.usgs.gov/monitoring-location/08324000/#dataTypeId=continuous-00060-0&showMedian=false&startDT=2021-04-01&endDT=2023-05-24 (accessed 15 May 2023).

Vuataz, F. and Goff, F., 1986, Isotope geochemistry of thermal and nonthermal waters in the Valles Caldera, Jemez Mountains, northern New Mexico: Journal of Geophysical Research, v. 91, p. 1835–1853. https://doi.org/10.1029/JB091iB02p01835

Vuataz, F., Goff, F., Fouillac, C., and Calvez, J., 1988, A strontium isotope study of the VC-1 core hole and associated hydrothermal fluids and rocks from Valles Caldera, Jemez Mountains, New Mexico: Journal of Geophysical Research, v. 93, p. 6059–6067. https://doi.org/10.1029/JB093iB06p06059

Wassenaar, L.I., Ahmad, M., Aggarwal, P., van Duren, M., Pöltenstein, L., Araguas, L., and Kurttas, T., 2012, Worldwide proficiency test for routine analysis of δ^2H and $\delta^{18}O$ in water by isotope-ratio mass spectrometry and laser absorption spectroscopy: Rapid Communications in Mass Spectrometry, v. 26, no. 15, p. 1641–1648. https://doi.org/10.1002/rcm.6270

Wilgus, J., Schmandt, B., Maguire, R., Jiang, C., and Chaput, J., 2023, Shear velocity evidence of upper crustal magma storage beneath Valles Caldera: Geophysical Research Letters, v. 50. https://doi.org/10.1029/2022GL101520

Appendices can be found at
https://nmgs.nmt.edu/repository/index.cfml?rid=2025003